2011

Applicability of Nanofluids in High Flux Solar Collectors

R. A. Taylor

P. E. Phelan

Todd Otanicar
Loyola Marymount University, totanicar@lmu.edu

C. A. Walker

M. Nguyen

See next page for additional authors

Recommended Citation

Taylor, R.A., Phelan, P.E., Otanicar, T.P., Walker, C.A., Nguyen, M., Trimble, S., and Prasher, R., 2011, "Applicability of Nanofluids in High Flux Solar Collectors," Journal of Renewable and Sustainable Energy, 3(2).

Applicability of nanofluids in high flux solar collectors

Robert A. Taylor,[1] Patrick E. Phelan,[1] Todd P. Otanicar,[2] Chad A. Walker,[1] Monica Nguyen,[1] Steven Trimble,[1] and Ravi Prasher[1]
[1]*Arizona State University, Tempe, Arizona 85287-6106, USA*
[2]*Loyola Marymount University, Los Angeles, California 90045, USA*

(Received 5 August 2010; accepted 28 February 2011; published online 1 April 2011; corrected 7 April 2011)

Concentrated solar energy has become the input for an increasing number of experimental and commercial thermal systems over the past 10–15 years [M. Thirugnanasambandam *et al.*, Renewable Sustainable Energy Rev. **14** (2010)]. Recent papers have indicated that the addition of nanoparticles to conventional working fluids (i.e., nanofluids) can improve heat transfer and solar collection [H. Tyagi *et al.*, J. Sol. Energy Eng. **131**, 4 (2009); P. E. Phelan *et al.*, Annu. Rev. Heat Transfer **14** (2005)]. This work indicates that power tower solar collectors could benefit from the potential efficiency improvements that arise from using a nanofluid working fluid. A notional design of this type of nanofluid receiver is presented. Using this design, we show a theoretical nanofluid enhancement in efficiency of up to 10% as compared to surface-based collectors when solar concentration ratios are in the range of 100–1000. Furthermore, our analysis shows that graphite nanofluids with volume fractions on the order of 0.001% or less are suitable for 10–100 MW_e power plants. Experiments on a laboratory-scale nanofluid dish receiver suggest that up to 10% increase in efficiency is possible (relative to a conventional fluid)—if operating conditions are chosen carefully. Lastly, we use these findings to compare the energy and revenue generated in a conventional solar thermal plant to a nanofluid-based one. It is found that a 100 MW_e capacity solar thermal power tower operating in a solar resource similar to Tucson, AZ, could generate ~$3.5 million more per year by incorporating a nanofluid receiver.
 [doi:10.1063/1.3571565]

I. INTRODUCTION

Due to its attractive economics and the possibility of storage, solar thermal energy is garnering significant interest and investment.[1] In order to deliver high quality energy to make electricity, sunlight must be efficiently concentrated, absorbed (i.e., converted to heat), and delivered to a thermal plant. This paper will discuss the feasibility of using a directly absorbing nanofluid to improve the efficiency of the receiver—a critical part of the system.

The basic concept of using particles to collect solar energy was studied in the 1970s by Hunt[2] and Abdelrahman *et al.*,[3] who mixed particles into a gaseous working fluid. In the past 10 years or so, particle receivers have been extensively modeled and several prototype collectors have been built and tested.[4–17] However, most of this work was devoted to finding reversible chemical reactions (many times in a gas phase) to generate hydrogen or some other chemical fuel. This study, on the other hand, examines direct conversion of light energy to useful *heat* by mixing small amounts of nanoparticles (<1% by volume) with a conventional base *liquid*.

Nanoparticles provide the following possible advantages in solar power plants: (1) the extremely small size of the particles ideally allows them to pass through pumps and plumbing without adverse effects, (2) nanofluids can absorb energy directly—skipping intermediate heat transfer steps, (3) the nanofluids can be optically selective (i.e., high absorption in the solar range and low emittance in the infrared), (4) a more uniform receiver temperature can be achieved inside

the collector (reducing material constraints), (5) enhanced heat transfer via greater convection and thermal conductivity may improve receiver performance,[3–17] and (6) absorption efficiency may be enhanced by tuning the nanoparticle size and shape to the application.[18]

The co-authors have shown (theoretically and experimentally) that in low-temperature solar collectors ($<100\ ^\circ$C) efficiency can be improved by using nanofluids.[18–20] This paper will extend that concept to a high-temperature nanofluid solar thermal collector. The central questions of this study are as follows. Is it possible to achieve these enhancements without adversely affecting other parts of the system (pumping costs or too much addition capital expense)? Furthermore, for a given conceptual design, what (if any) improvement is expected compared to a conventional solar thermal collector? To answer these, comparisons are made using numerical modeling of the radiative transfer equation as presented in Sec. II. These questions are also explored through experimentation on a small nanofluid dish collector. A simple economic analysis is conducted to illustrate the implications of using a nanofluid collector.

II. THE NANOFLUID SOLAR COLLECTOR

Since there are no commercial nanofluid solar collectors yet, this section will outline our assumptions, reasoning, and choices made in designing one. As mentioned above, nanofluids are a mixture of very small-sized particles and the conventional liquids used in a given application. Therefore, the first design choices to be made are in selecting those two components. Common base liquids in solar collectors are water, heat transfer oil, or molten salt. The choice between these liquids is usually determined by the required operating temperatures. Heat transfer oils are commonly used for medium temperature ranges ($100\ ^\circ\text{C}-400\ ^\circ\text{C}$), which are suitable for Rankine thermal cycles, and are our choice for this study. For efficient solar collection, the particles need to be highly absorptive, which limits our study to metallic and graphite particles. We will further limit our options by only selecting particles that are widely available "off-the-shelf" and are thus made in larger production volumes. For instance, some nanopowders can now be found for around \$1000/kg.[21] Of course, gold, platinum, palladium, and other precious metals fit this criterion but are not cost-effective. (Note: all \$ amounts are given in 2011 U.S.\$. Note also that gold nanopowder is $\sim\$190/\text{g}$ or about five times its bulk price).

The volume fraction of nanoparticles in the base fluid must be chosen carefully to get the most out of a nanofluid. If the nanoparticle concentration is too high, all the sunlight will be absorbed in a thin layer near the surface of the receiver—i.e., not volumetrically. If the concentration is too low, a significant portion of the light will be transmitted out of the fluid. Ideally, the least amount of particles needed to effectively absorb light will be used to minimize cost. It should also be noted that much research has gone into finding additives and treatments (*p*H buffers, surfactants, chemical treatments, etc.) that will create a stable nanofluid.[22,23] Therefore, we will assume here that it is possible to attain a nanofluid that has a long-term stability.

For simplicity, we will set scale boundaries by considering two plant sizes—10 and 100 MW_e. This range is used in order to analyze utility scale power systems and also to stay in a range where they might feasibly be built, or retrofitted, in the near term. Trough (i.e., linear focus) systems are a poor choice for nanofluids because a relatively large amount of surface area would require modification. This study will consider only relatively high concentration (i.e., spot focus) schemes of solar thermal electrical generation. This choice was made to ensure that the change from conventional to nanofluid receiver would require only small changes in materials when compared to the entire solar collection system. Figure 1 gives two notional designs of a potential nanofluid receiver—designated as A and B. Raw materials needed for this design are steel, high-temperature insulation, and possibly glazing [e.g., antireflective float glass—see TECHSPEC™ from Edmund Optics Inc., 101 East Gloucester Pike, Barrington, NJ 08007-1380, USA[24]]. Receiver A (with glazing) could be oriented vertically or horizontally and operated at pressures well above ambient. Ideally, the cold inlet stream could be directed toward the glazing to improve efficiency and to lance nanoparticles off the glazing to preserve transparency. Receiver B could work in a beam-down concentrator under atmospheric pressure since the fluid is not confined. Receiver B could also be turned on its side where the fluid flow would be a falling film. The

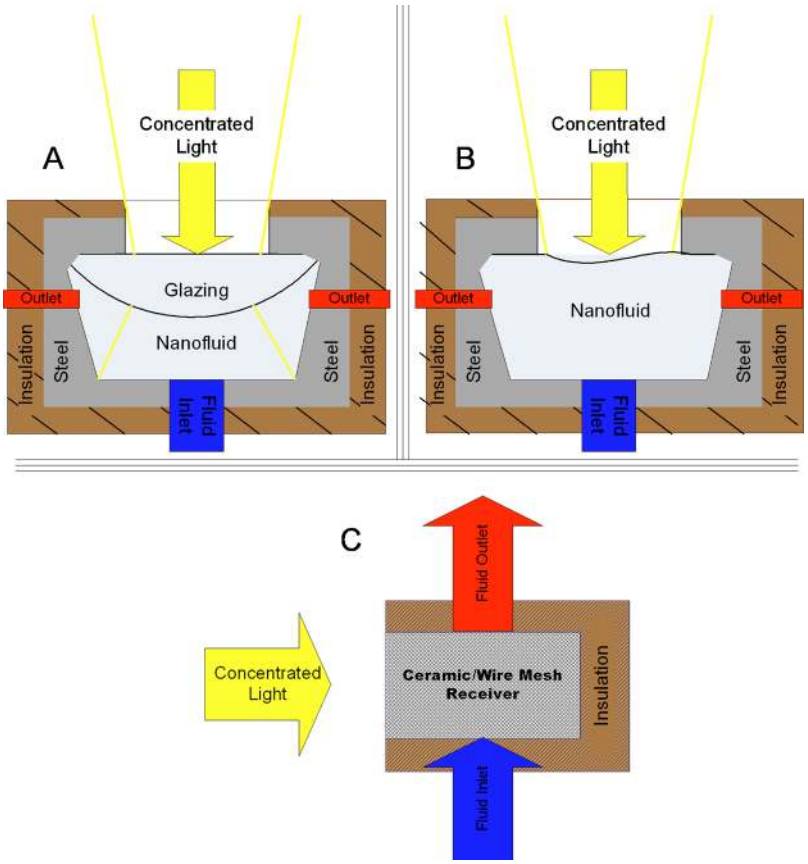

FIG. 1. (a) Conceptual design of a nanofluid concentrating collector with glazing. (b) Conceptual design of a nanofluid concentrating collector without glazing. (c) Conceptual drawing of a conventional power tower solid surface absorber.

advantage of receiver B is that it could avoid the reflective losses of the glazing. Lastly, Fig. 1(c) gives a simplified schematic of a conventional power tower solid surface absorber. The conventional power tower receiver is composed of a wire/ceramic mesh used to absorb energy over a finite depth. This type of receiver is sometimes referred to as volumetric absorber, but it must still transfer heat through a solid surface via conduction and convection to the working fluid. That is, the energy must go through at least one intermediate heat transfer step. Figure 2 compares the heat transfer process of a surface-based collector and a volumetric-based collector in terms of their thermal resistance networks. According to this simple model, with all things being equal, a volumetric receiver should provide less resistance in converting sunlight into useful heat.

There are several interesting differences between a conventional receiver and our conceptual nanofluid receiver. (1) The nanofluid receiver may unavoidably require a transparent glazing to contain high-temperature/pressure fluid; however, the glazing material *could* be shaped to employ secondary optics. (2) The nanofluid, by skipping a conduction/convection heat transfer step, could avoid a significant temperature drop and some heat loss. (3) The nanofluid receiver may require more maintenance and/or a somewhat higher capital expenditure. (4) An equivalent solar collector must have more tightly controlled optics, flow conditions, and receiver geometry. (5) Finally, thermal/optical properties and thus receiver efficiencies are expected to be different from a surface absorber—this is modeled in Secs. III–VII

III. NANOFLUID OPTICAL PROPERTIES

To determine how a large-scale solar collector might perform without actually building it, we must employ a model. For this paper, a general nanofluid model developed by the co-authors, as

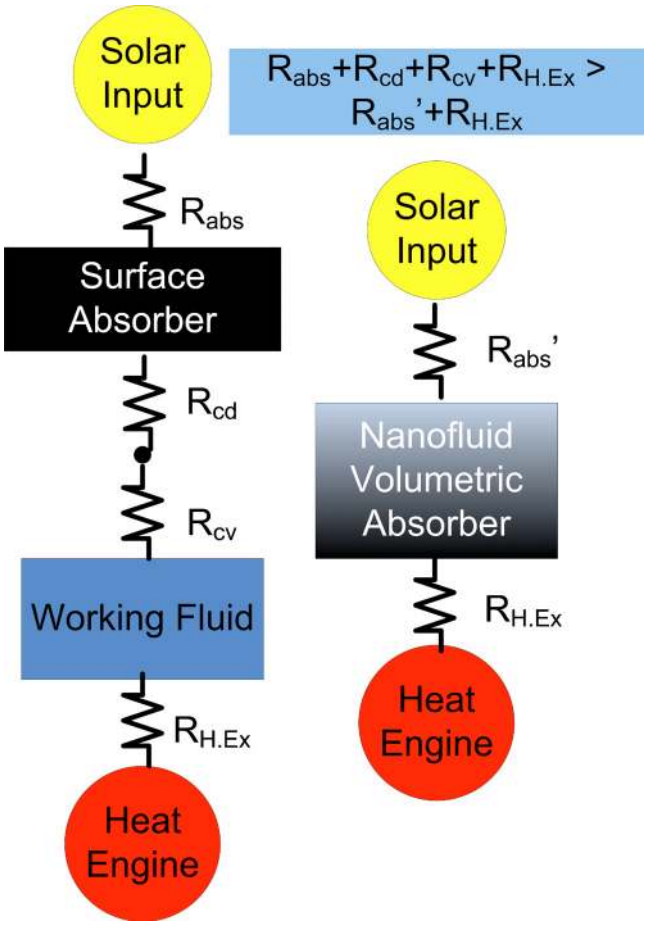

FIG. 2. Thermal resistance network—comparison between a conventional solar thermal plant and a nanofluid solar thermal plant. R_{abs}, R_{cd}, R_{cv}, $R_{H.Ex}$, and $R_{abs'}$ refer to the thermal resistance of solid surface absorption, conduction, convection, fluid-to-fluid heat exchange, and volumetric solar absorption heat transfer steps, respectively.

described in Ref. 18, is used. The model is a coupled solution of the radiative transfer equation and energy equation and is briefly described in Sec. IV. In short, the optical properties of small particles (which are relatively far apart) can be found without too much difficulty. After some calculation, the extinction coefficient, $\sigma_{e,\lambda}$, can be found such that

$$\sigma_{e,\lambda} = f(\tilde{n}_{\text{bulk}}, \tilde{n}_f, D_p, \lambda, f_v). \tag{1}$$

That is, $\sigma_{e,\lambda}$ is a function of the complex refractive index, $\tilde{n}_{\text{bulk}}$, of the bulk particle material, the complex refractive index of the base fluid, $\tilde{n}_f$, particle size, D_p, wavelength, λ, and the volume fraction, f_v. Commonly available nanoparticles are in the range of 10–100 nm.[21] For this study, we will assume 20 nm average diameter particles to limit the number of variables. A synthetic heat transfer fluid commonly used in solar systems, Therminol VP-1 (a eutectic mixture of 73.5% diphenyl oxide and 26.5% biphenyl[25]), is used as the base fluid in this analysis because of its ability to remain liquid at elevated temperatures. Also, we have limited our analysis to aluminum, copper, graphite, and silver nanoparticles. With the exception of silver, these materials are relatively cheap and have a high complex component of the refractive index—i.e., their extinction coefficients are proportionally high. Silver was also chosen because it has a very high absorption peak (due to plasmon resonance) near sunlight's peak irradiance.

Using these assumptions, extinction coefficients versus wavelength are plotted for selected nanofluids in Fig. 3. Note that volume fractions were chosen to absorb >90% of incoming solar

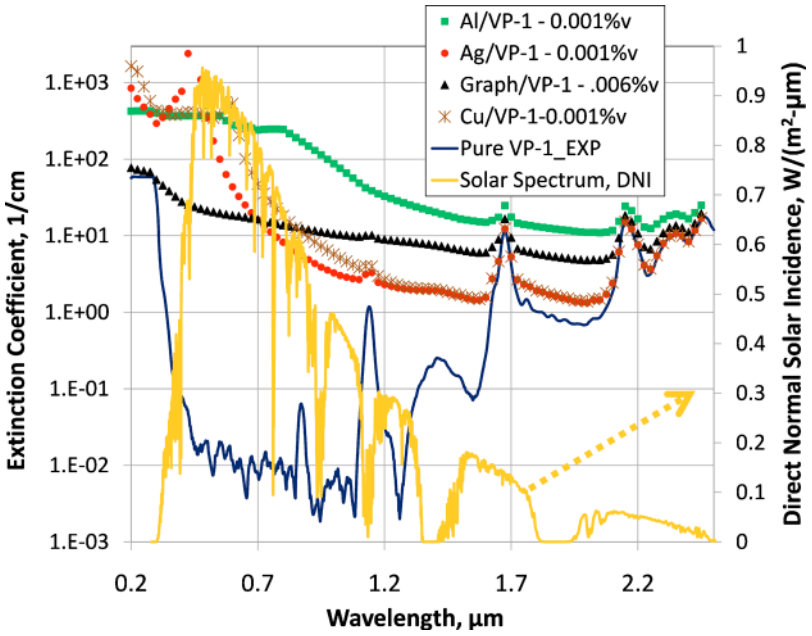

FIG. 3. Extinction coefficient over the visible range for copper, graphite, silver, and gold—$D=20$ nm, $f_v=0.1\%$. The "Pure VP-1_ EXP" is an experimental result for the pure base fluid, Therminol VP-1—as found with a Jasco V-670 spectrophotometer.

power in a receiver depth of 5 cm. These results also take into account the fact that the size of these particles is on the order of the mean free path size of electrons. That is, we must account for the fact that we are using bulk material properties for nanoscale materials. A simple Drude model, as described in Ref. 18, is used to change the optical properties by adding in a damping coefficient to electron oscillations—dependent on the particle size. Essentially, this added step broadens the absorption peaks for small particles (and slightly lowers them).

One major loss of energy in the receiver is from reflections from the surface of the absorbing fluid. In order to make sure that this is not a major drawback, we modeled the reflectivity using the Maxwell Garnett effective medium theory. Next, reflectance at the fluid interface (simplified for normal incident light) can be found. The following equations are used:[26]

$$\frac{\varepsilon_{\text{eff}}-\varepsilon_f}{\varepsilon_{\text{eff}}+2\varepsilon_f}=f_v\frac{\varepsilon_p-\varepsilon_f}{\varepsilon_p-2\varepsilon_f}. \tag{2}$$

In this expression, ε and f_v are the dielectric constant and the volume fraction, respectively, where the subscripts eff, f, and p define the effective medium (what we are solving for), the fluid, and the particles, respectively. Once we know the properties for the effective medium, we can apply the following Fresnel equation to estimate reflectance (assuming light is near normal incidence):[26]

$$\Re=\frac{(\tilde{n}_{\text{eff}}-\tilde{n}_{\text{air}})^2}{(\tilde{n}_{\text{eff}}+\tilde{n}_{\text{air}})^2}. \tag{3}$$

In this expression, $\tilde{n}$ is the refractive index and $\Re$ is used to represent reflectance and distinguish it from thermal resistance, R. Also, the subscripts eff and air denote the effective nanofluid and air, respectively. It should be noted that any variation due to temperature is neglected in these calculations.

These reflectance results are compared in Fig. 4 to a selective surface absorber. These results show that according to our model, an unglazed nanofluid receiver would actually lose less of the incoming radiation to reflections than a selective coating. Note that the nanofluid materials have

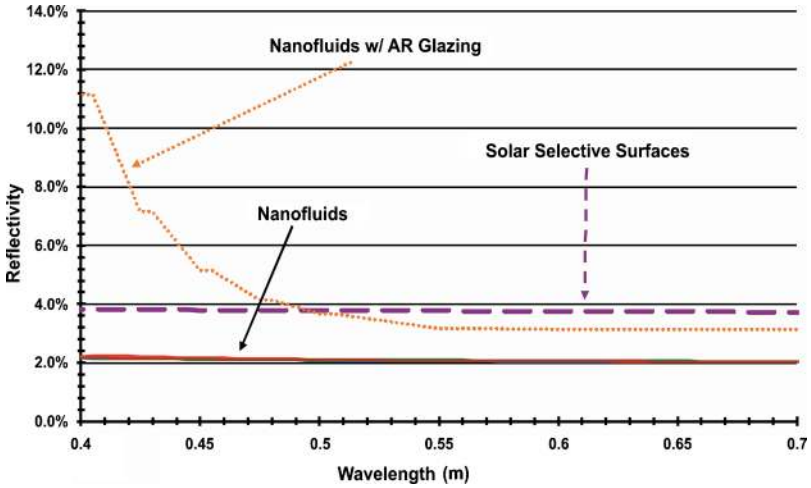

FIG. 4. Reflectivity as a function of the wavelength of copper, graphite, silver, and gold (20 nm) nanofluids with a volume fraction of 0.1% and (w/ and w/o) glazing as compared to that of a conventional selective surface absorber (Ref. 27).

essentially coincident curves over the solar spectrum in Fig. 4. Nanofluid thermal emission, however, is much higher than a selective surface—especially for graphite. This means that adding a glazing that traps long-wavelength infrared emission would be advantageous. Hence, glazing gives a slight increase in total reflection over the whole spectrum (compared to a selective surface), but the reduction in radiative losses easily make up for it.

Of course, these reflective losses are only a part of the optical losses that add up to derate solar receivers. Dust, optical aberrations, limitations in the mirrors, etc., will most likely add to account for a large share of the losses in optical efficiency. System optical efficiencies are usually, at best, 80%–90% for new, clean optics.[28]

IV. NANOFLUID RECEIVER MODEL DESCRIPTION

After the optical properties are found, we can numerically approximate the efficiency of a solar receiver. This is done, as illustrated in Fig. 5, by assuming that concentrated light enters from the top of the receiver where it is absorbed/scattered, converted to heat, and carried out by a flowing nanofluid. Some of the light energy is lost to reflection, while heat is lost on the boundaries of the receiver due to convection and radiation. A characteristic temperature field inside the receiver is also shown in Fig. 5.

Absorption of light is modeled inside the receiver with the following one-dimensional radiative transport equation:[26]

$$\frac{dI_{i,\lambda}}{dy} = \sigma_{a,\lambda} I_{b,\lambda}(T(y)) - \sigma_{e,\lambda} I_{i,\lambda}, \tag{4}$$

where $\sigma_{a,\lambda}$ is the spectral absorption coefficient. The subscript i is used to keep track of which direction light is propagating—i.e., either incoming (+1) or outgoing (−1) light. As described in Ref. 29, the boundary conditions are as follows:

$$I_{-1,\lambda}(L) = \varepsilon_{w,\lambda} I_{b,\lambda}(T(L)) + \rho_{w,\lambda} I_{+,\lambda}, \tag{5}$$

$$I_{+1,\lambda}(0) = S_\lambda + \rho_{g,\lambda} I_{-1,\lambda}(0). \tag{6}$$

For these equations, we need to know the spectral reflectance of the wall and the glazing, $\rho_{w,\lambda}$ and $\rho_{g,\lambda}$, respectively, and the spectral radiation incident on the receiver, S_λ. The spectral wall emittance, $\varepsilon_{w,\lambda}$, is also needed. We also assume incoming light to be blackbody radiation,[26]

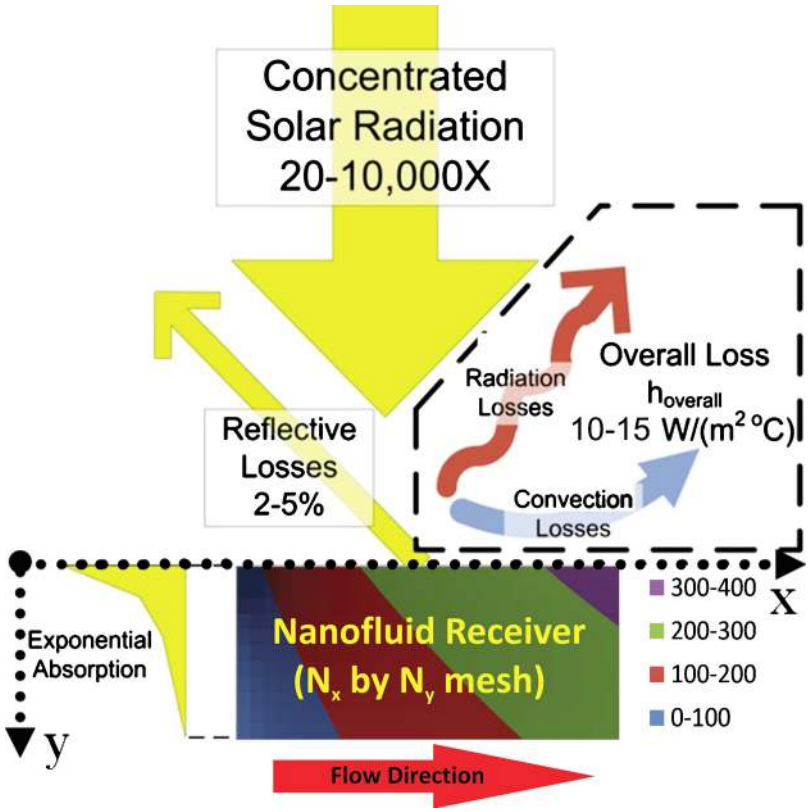

FIG. 5. Schematic of conditions used in the numerical model with a characteristic temperature field shown.

$$I_\lambda(T) = \frac{2hc_0^2}{\lambda^5\left[\exp\left(\frac{hc_0}{\lambda k_B T}\right) - 1\right]}, \tag{7}$$

where h is the Planck's constant, k_B is the Boltzmann's constant, and c_0 is the speed of light. To model the temperature profile, we couple the above equations with the following two-dimensional energy equation and its boundary conditions. The equations necessary for this model are as follows:[26]

$$k\frac{\partial^2 T}{\partial y^2} - \frac{\partial q_r}{\partial y} = \rho c_p U \frac{\partial T}{\partial x}, \tag{8}$$

$$x = 0, \quad 0 < y < L, \quad T(0,y) = T_{\text{inlet}},$$

$$y = L, \quad x > 0, \quad q_r(L) - k\left.\frac{\partial T}{\partial y}\right|_{y=L} = 0, \tag{9}$$

where k, ρ, c_p, and U are the fluid thermal conductivity, density, specific heat, and velocity, respectively. To simplify the model, the velocity profile is assumed constant—i.e., plug flow. Furthermore, we also assume an overall loss coefficient (which combines convection and radiation) at the boundary to be in the range of 10–15 W m^{-2} C^{-1}—depending on the fluid temperature. Finally, we shall define receiver efficiency as[26]

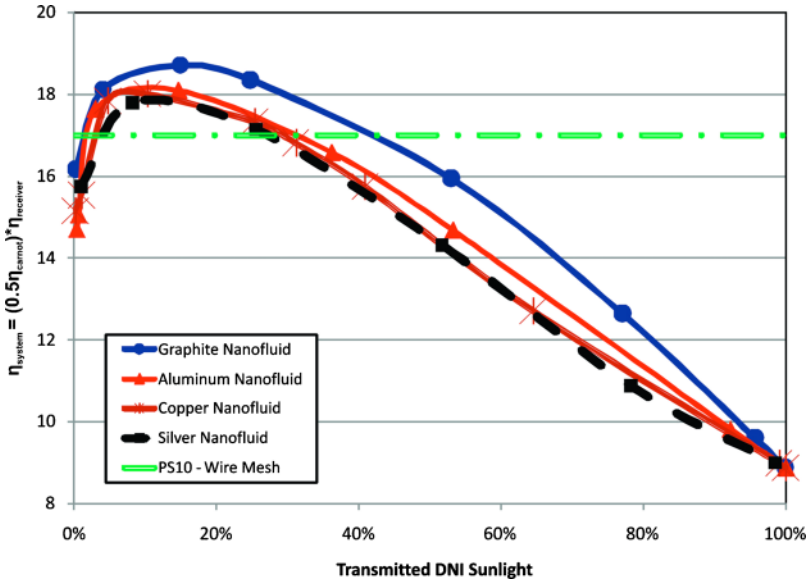

FIG. 6. Modeled system efficiencies of graphite, copper, aluminum, and silver nanofluids with the system efficiency of Abengoa's PS10 solar power tower for comparison (Ref. 30).

$$\eta_{\text{rec}} = \frac{\dot{m}c_p(T_{\text{out}} - T_{\text{in}})}{CG_T A_R}, \tag{10}$$

where $\dot{m}$, c_p, T_{out}, T_{in} are the mass flow rate, specific heat, and outlet and inlet temperatures of the fluid, respectively. Also, C, G_T, and A are the concentration ratio, the solar irradiance, and the collector area, respectively. It should be noted that G_T is calculated from the results of Eq. (7). The interested reader can find more details on this model (developed by the co-authors) in Refs. 18 and 19.

V. NANOFLUID RECEIVER AND SYSEM MODEL RESULTS

Once the general model is developed, it is simply a matter of conducting a parametric study to examine how the solar receiver and power plant system efficiencies vary. In the following analysis, we have chosen to study the following important independent variables: particle material, particle volume fraction, mass flow rate, and solar concentration ratio.

First, we will compare our chosen nanofluids while holding mass flow rate and solar concentration ratio constant—at 180 kg/s and 620 suns, respectively. Another important parameter that must be chosen is the reflectivity of the backing material, which, in this case, was milled aluminum, $\Re_{\text{av}} \sim 0.5$, to match with the experimental work described in the following sections. For these conditions, Fig. 6 plots the system efficiency versus the percent of transmitted direct normal irradiance—i.e., versus the total percent of solar power left after one pass through the nanofluid. System efficiency, as noted in the figure, is defined as follows:

$$\eta_{\text{system}} = 0.5\left(1 - \frac{T_c}{T_H}\right)\eta_{\text{rec}}. \tag{11}$$

Equation (11) multiplies the receiver efficiency, η_{rec}, by a Carnot heat engine and which runs at 50% efficiency.

Figure 6 shows that minor differences of less than 2% in system efficiencies are obtained with different nanofluids for comparable sunlight absorption. The differences that are present in system efficiency presumably result from spectral differences in the nanofluid's extinction coefficient and scattering. For example, the extinction coefficient of graphite comes almost entirely from absorp-

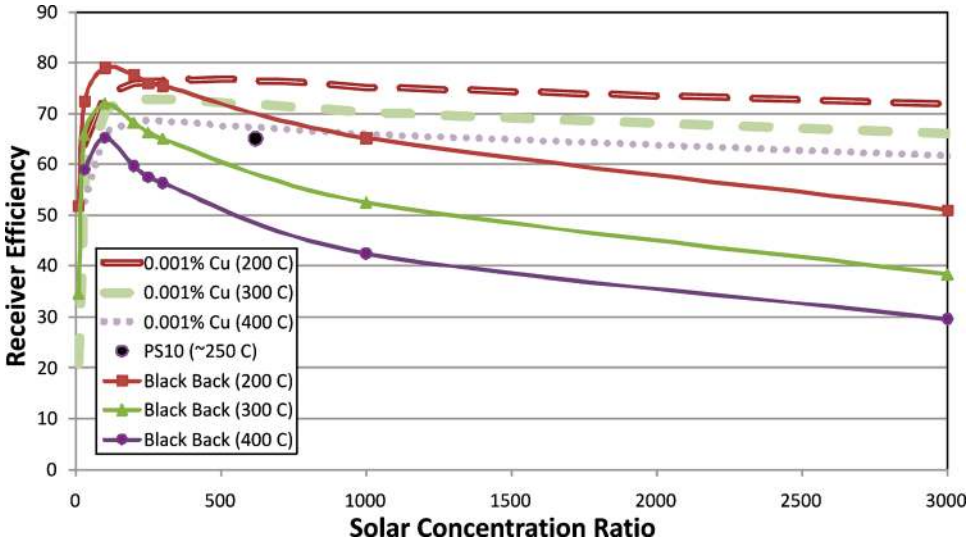

FIG. 7. Modeled receiver efficiency as a function of concentration ratio, with f_v=0.1%, A_R=264 m^2: Single points—published values (Ref. 30).

tion, $\sigma_{a,\lambda} \approx \sigma_{e,\lambda}$. That is, graphite scatters very little incident light and thus it has a slightly higher system efficiency for most conditions. In addition, graphite has a relatively uniform extinction coefficient as a function of wavelength, which also separates it from the metals. Figure 6 also shows that there is an optimum nanoparticle volume fraction for each fluid which will achieve maximum system efficiency. In this analysis, the optimum point occurs when 85%–95% of the incident light is absorbed on the first pass with most of the remainder being absorbed on the semiabsorbing back or as reflected light goes back up through the fluid. In general, absorbing the light *away* from the boundaries—where heat can be lost—provides the best result. The exact nanoparticle volume fraction, however, should be found for individual applications as it depends on parameters such as flow rate, solar irradiance, heat loss conditions, reflectivity of the backing material, receiver geometry, and ambient conditions.

As a baseline case, the receiver geometry and approximate operating conditions (i.e., geometry and concentration ratio range) are fixed to be roughly comparable to Abengoa's PS10 power tower in Seville, Spain.[30] Under normal conditions, the PS10 produces about 55 MW thermal power (~11 MWe) with 250 °C steam at 40 bars,[30] which is roughly similar to the nanofluid results. To highlight the comparison between our nanofluid model and the PS10 power plant, its system efficiency is plotted as a straight line in Fig. 6. In the end, the cheapest, stable nanofluid should be the choice for a solar thermal power plant. According to our analysis, in a large-scale system this is likely graphite (at nearly \$1/g in bulk[21]) with a volume fraction on the order of 0.001% or less. It should be noted, however, that the price difference between nanoparticles may be negligible with respect to system capital costs.

Now, we shall consider the effect of varying the solar concentration ratio and the mass flow rate while holding particle material and volume fraction constant. Figure 7 shows receiver efficiencies as a function of solar concentration ratio. In order to meet 200, 300, and 400 °C outlet temperature constraints, a proper mass flow rate must be found by running the model several times to find each data point. It should be noted that in most cases flow rates end up being in the fully turbulent regime—i.e., Reynolds numbers ranging from 1×10^5 to 1×10^6. However, pumping power from frictional losses is calculated to be negligible (less than 1% of the power plant's electrical output) since the receiver length is relatively short. Also, an upper limit on temperature was imposed since our base fluid, Therminol VP-1, cannot operate (as a liquid) above 400 °C. In

this analysis, 0.001% volume fraction copper nanofluids were chosen based on their approximate optimum point in Fig. 6. (Note: graphite will be modeled and compared against the experimental results in Sec. VI.)

Figure 7 also shows model results for the pure base fluid (i.e., nearly nonabsorbing) with a selective surface "black backing" under similar receiver operating conditions. The results in Fig. 7 illustrate that a nanofluid collector may operate more efficiently than a conventional surface solar collector under optimum conditions—up to 10% higher for solar concentration ratios in the range of 100–1000. As shown in the figure, the nanofluid and its operating conditions must be chosen carefully or the system may end up operating less efficiently. A nanofluid receiver could also potentially be useful in a direct steam generation system like those described in Ref. 28 but phase change was not modeled in this paper.

Figure 7 also indicates (for a given nanofluid type and receiver geometry) that a maximum efficiency is reached at a solar concentrations of about 275–300 (or $275-300\ \mathrm{kW/m^2}$ incoming solar flux). This maximum occurs as a slight positive function of the outlet temperature—e.g., a higher outlet temperature leads to peak efficiency occurring at a slightly higher concentration ratio. Again, these results are dependent on the many constant system parameters, but the trends should be similar for other designs.

VI. LABORATORY-SCALE NANOFLUID DISH COLLECTOR TESTING

In order to evaluate some of the predictions of this model, some experiments with a nanofluid dish collector were conducted. Previous work of the co-authors found that for low-temperature solar collectors the numerical model matches quite well with experimental data from a mini-flat-plate solar collector.[31] To explore higher temperature collectors, a dish collector was chosen. The dish was selected because it is easy to work with and because we were able to build the whole collector system cheaply. A tracking/mounting system was designed and built in a few weeks using a graciously donated parabolic dish from the Physics Laboratory of Lake Havasu. Although this laboratory-scale dish collector is not directly comparable to the large-scale results found above, we believe the relative comparison between a nanofluid volumetric receiver and its base fluid with a semiabsorbing backing is valuable as validation of the model. Also, we use a relative comparison to divide out the losses present in our experimental system.

The system is composed of three parts: the tracking system, the dish, and the receiver. The tracking system is controlled in one axis throughout the day by two photodiodes connected by a simple control circuit to a step-motor. The motors adjust when shade from a fin covers one of the photodiodes, which keeps the normal axis of the dish parallel to the sun. The second axis of the dish—the tilt angle—is adjusted manually.

The dish is made of polished aluminum and has an intercept area of $0.46\ \mathrm{m^2}$. The manufacturer-quoted average dish reflectivity is >90%—however, this reflectivity is for the ideal flat material—i.e., normal incidence in pristine condition. Thus, in our experiments we expect slightly lower reflectivity.

The receiver was machined from two separate blocks of aluminum, which are bolted together with glazing at the center. The thickness (i.e., depth) of the fluid flowing in the receiver is 1 mm. The experimental receiver design has double-paned, $2\ \mathrm{cm} \times 2\ \mathrm{cm}$, microscope slide glazing. In the modeling results above, the model only included a single pane of clean glazing. For simplicity, each additional glazing can be assumed to be another ~5% loss.

Figure 8 shows images of the dish and receiver used in these experiments. Removed from the receiver are the thermocouples (which measure the heat energy gain) and pressure probes (which determine the flow rate inside the receiver). Temperatures seen inside the receiver were up to 270 °C. Mass flow rates in the collector were on the order of $1 \times 10^{-4}\ \mathrm{kg/s}$, giving laminar Reynolds numbers of approximately 15–25 for all steady flow conditions.

The receiver backing was left as machined aluminum, which we assumed had a reflectivity around 0.5 since it was a dull finish. Tests with a reflected green laser indicated that this was a reasonable estimate. Furthermore, we know the aluminum backing absorbs about half of the incident light because tests with just the base fluid convert sunlight into heat at ~28% efficiency

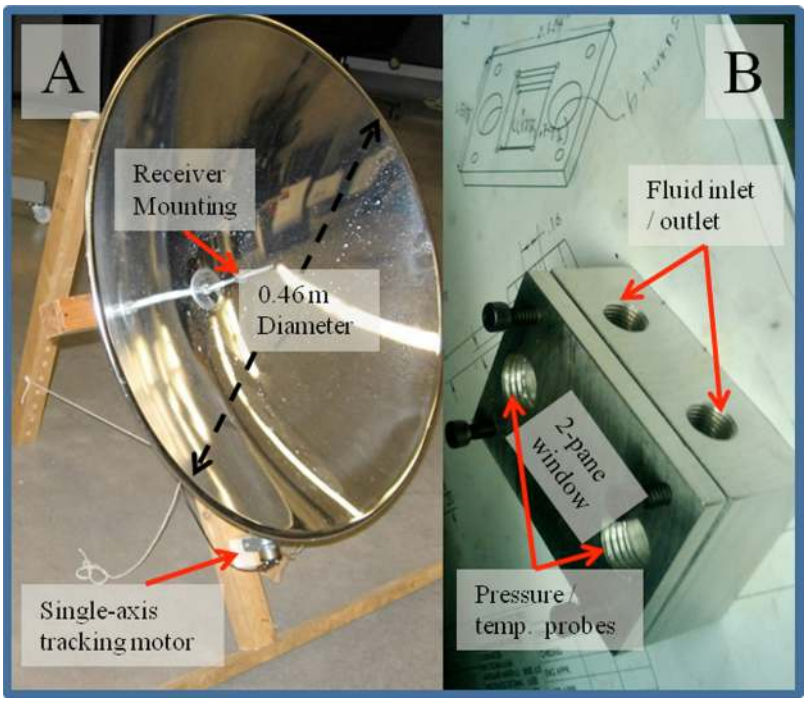

FIG. 8. (a) Laboratory-scale single-axis tracking, reflective dish. (b) Aluminum machined receiver with instrumentation ports.

in our experiments. Reflection off the front glazing, reflections from the aluminum backing transmitted out of the fluid, and heat losses presumably add to give base fluid efficiency of ~28%.

The base fluid used in these experiments is the same as that assumed in the model, Therminol VP-1 heat transfer oil.[25] Graphite nanoparticles were mixed into the Therminol oil since our analysis showed that they appear to be the cheapest and most efficient solar absorbers. The volume fractions used in this 1 mm deep channel are 0.125% and 0.25%. In these fluids, the particles will be closer to each other than the low volume fractions mentioned above, but we can still use the Rayleigh scattering approximation of the model. Also, in one pass (1 mm) through the collector, these volume fractions are expected to absorb >90% of the incoming solar spectrum, which is very similar to the modeling results above.

The dish collector has a geometric concentration ratio of ~400, which is very near the optimum concentration ratio of Fig. 7. This concentration ratio is calculated using the measured intercept area of the dish and dividing by the measured spot size (found using burn paper). During testing, the dish experienced direct normal irradiances of 800–950 W/m^2 [Tempe, AZ—from NREL (Ref. 32)]. It should also be noted that data of the global irradiance were also recorded periodically during the experiments. For this, a pyranometer from Matrix, Inc., 537 S. 3 1st, Mesa, AZ 85204, USA (an MK 10 Sol-A-Meter) was used to confirm the data from NREL.[32] At its peak the nanofluid dish tracker achieved a maximum solar-to-thermal energy conversion efficiency of ~34% at outlet temperatures ~250 °C. This is about 20% higher than the receiver with the Therminol oil alone under similar conditions. Figure 9 shows the steady-state efficiencies achieved in these experiments. Since we did not know the exact optical efficiency for the dish collector (e.g., spectral reflectivity of the dish and other components as well as shadowing from components), efficiencies are plotted as a ratio of the nanofluid steady-state thermal efficiency to the base fluid's steady-state efficiency under similar conditions. Figure 9 shows these results with error bars determined by a simple error propagation analysis.

These experiments indicate that nanofluids can only provide an advantage if the composition is chosen carefully and the fluid/tracking system is precisely controlled. For higher volume frac-

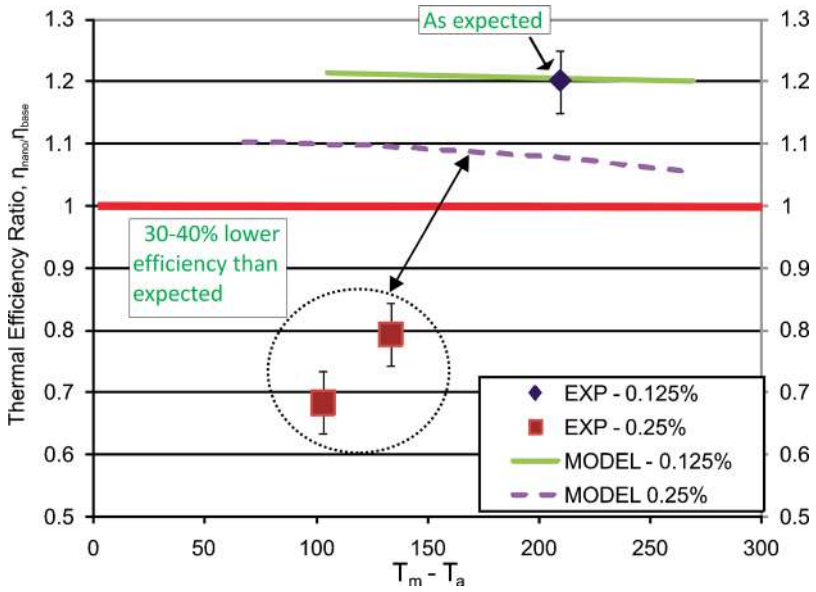

FIG. 9. Normalized steady-state efficiencies for conventional collectors (lines) compared to our outdoor laboratory-scale dish experiments (data points).

tions >0.125%, we had a difficult time achieving relative efficiencies near what the model predicted. One possible reason for poor results is that the nanofluids were unstable (i.e., the particles agglomerate, become large/heavy and settle out) at higher volume fractions. Another possible reason is that in a more concentrated nanofluid light will be absorbed in a thin upper layer of the fluid where it can easily transfer back out of the receiver. While the model should predict thermal emission for an ideal, stable nanofluids, significant deviations are possible with high solar fluxes if particle agglomeration occurs. On the other hand, for lower volume fractions, our experiments found significant efficiency improvements that matched quite well with the model. A 0.125% volume fraction of graphite resulted in approximately an 11% improvement in steady-state efficiency over the base fluid.

Overall, our limited preliminary data show that similar efficiency improvements are possible in when the fluid is chosen and controlled carefully. However, if the nanofluid becomes unstable or if tracking is inaccurate, a nanofluid collector can become very inefficient indeed.

VII. ECONOMIC IMPLICATIONS

It is estimated that less than 30 or 300 kg of nanoparticles would be needed in a 10 or 100 MW_e solar thermal power plant, respectively. Thus, at a nanoparticle price of ~$1000/kg (Ref. 21) (as mentioned above), the cost increase of using a nanofluid would still be less than 0.1% of the total plant capital investment—assuming $5/W.[33] The cost of changing receivers was not estimated, but no exotic materials or fabrication methods would be needed to produce a large-scale nanofluid receiver. In fact, a receiver made of antireflective glass, steel, and insulation may actually be cheaper than a ceramic mesh receiver. It should be noted that operation and maintenance costs are more difficult to estimate. We believe (from the observation of stagnant nanofluids stored in glass containers for up to 18 months) that very little extra maintenance would be required inside a nanofluid receiver in the short term. That is, a properly prepared nanofluid in a closed loop could be relatively stable and should not need replacement. Good design, operation, and maintenance (with occasional cleaning) could keep interior surfaces transparent and free from particle deposits. A closed system should also prevent any added environmental costs during the nanofluid's use phase. However, long-term studies have not been conducted and nanofluid leak/spill prevention and/or clean-up could be costly. For instance, remixing of the nanofluid and cleaning of optical

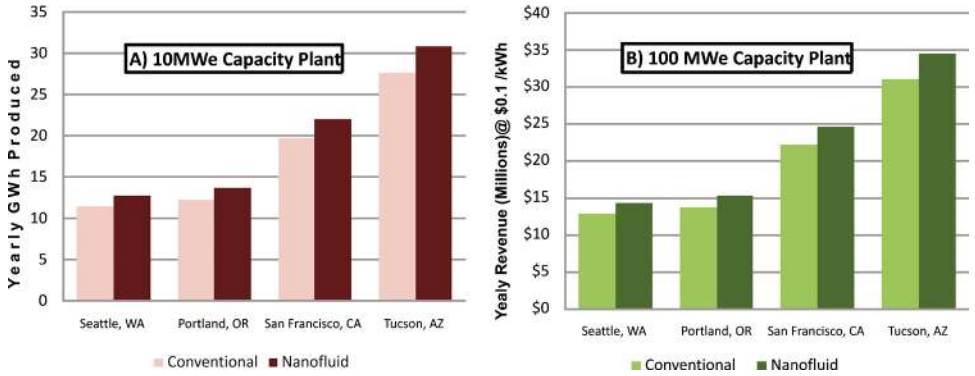

FIG. 10. (a) Comparison of yearly electricity generation for a plant rated at 10 MW_e. (b) Comparison of the estimated revenues for a 100 MW_e commercial scale plant.

surfaces may be necessary on a regular basis, which could require specialized equipment. Expenses beyond the initial capital investment are not estimated in this study.

For simple economic comparison, we will conservatively assume that an optimized nanofluid receiver can be about 5% more efficient than a conventional one. To demonstrate the advantage of this small change, Fig. 10(a) gives a comparison of yearly electricity generation between a conventional power plant with the characteristics of Abengoa's PS10 and a similar plant with a nanofluid receiver. That is, both receivers have a solar concentration ratio, 620, receiver area, 265 m^2, outlet temperature, 250 °C, and power block efficiency, 27%, similar to the PS10.[30] Both systems assume a capacity factor of 85% for the solar resource available at the given locations in Fig. 10. In other words, we conservatively assume that maintenance or other factors will take the plant out of service for 15% of the sunny hours. Thus, the only difference between the two systems is that the receiver is operating 5% more efficiently.

The locations in Fig. 10 were chosen because they cover a wide range of solar resource conditions. As such, the results range from Seattle, WA, to Tucson, AZ, which, on the average, receive 2.9–7 kW h/m^2 of direct normal incident solar energy per day—as given by NREL for 2-axis trackers.[32] Comparison of different locations merely demonstrates that any enhancement from a nanofluid receiver would become even more advantageous for areas with higher incoming solar energy.

Figure 10(b) puts the comparison in monetary terms (assuming sale of electricity at 10 cents/kW h) and scales it up to a 100 MW_e, commercial-sized plant. Again, a conservative power block efficiency of 26% was used, but for the larger scale plant, we assume that 90% of the solar resource could be utilized. Even with conservative assumptions, this kind of enhancement adds nearly $3.5 million to the yearly revenue of a large plant—which could take about two years off the simple payback time of the plant (assuming $5/W, installed[33]). If peak prices and carbon credits are taken into account, a nanofluid receiver would look even more attractive.

VIII. CONCLUSIONS

Overall, the goal of this paper was to conduct a conservative, simplified analysis of how a nanofluid-based concentrating solar thermal system would compare to a conventional one. Based on the results of this study, nanofluids have excellent potential for power tower solar thermal power plants. Efficiency improvement on the order of 5%–10% is possible with a nanofluid receiver. Ideally, these enhancements could be realized with very little change (in terms of materials, system design, and initial capital investment) to the entire solar thermal system.

Fundamental differences in volumetric absorption versus solid surface absorption drive this enhancement in thermal efficiency for a power tower solar plant. It should be noted, however, that nanofluids are not expected to be suitable for dish or trough solar thermal systems at this time, but further optimization (or cost reductions) might expand their range of applicability. In this study, a

particular nanoparticle material, shape, and some characteristic operation temperatures were chosen using engineering judgment, but further optimization is possible. It is expected that additional improvements could be made by tailoring the optical and thermal properties of the nanofluid more closely to specific system conditions.

This paper also demonstrates that as solar thermal power plants move to larger scale (in good resource sites), nanofluid receivers show even more potential. A simple economic estimation shows that a 100 MW_e nanofluid thermal plant (operating in Tucson, AZ) could add $3.5 million to the yearly revenue of large-scale plants under favorable conditions.

ACKNOWLEDGMENTS

The authors gratefully acknowledge the support of the National Science Foundation through Award No. CBET-0932720.

Nomenclature

A	Area, m^2
c_p	Specific heat, J kg^{-1} $°C^{-1}$
c	Speed of light, m/s
C	Concentration ratio
d	Distance, m
D	Mean particle diameter, nm
f_v	Volume fraction, %
G	Incident solar flux, W m^{-2}
h	Heat transfer coefficient, W m^{-2} $°C^{-1}$
h	Planck's constant, m^2 kg/s
I	Irradiance, W m^{-2} nm^{-1}
k	Thermal conductivity, W m^{-1} $°C^{-1}$
k_B	Boltzmann's constant, m^2 kg s^{-2} K^{-1}
L	Length, m
m	Mass flow rate, kg s^{-1}
$\check{n}$	Complex refractive index
q''	Heat flux, W m^{-2}
R	Thermal resistance, °C/W
$\Re$	Reflectance
S	Spectral irradiance, W m^{-2}
T	Temperature, °C
U	Fluid velocity, m/s
x	Layer thickness, m
Y	Length, m

Subscripts

∞	Far away (ambient)
abs, a	Absorption
amb	Ambient
av	Average
bulk	Bulk properties
c	Cold
cd	Conduction
cv	Convection
e	Electric
e	Extinction
eff	Effective
f	Fluid
g	Glazing
h	Hot

H.Ex	Heat exchanger
I	Counter
in	Inlet
j	Incident
o	Outer
out	Outlet
P	Particle
ref	Reference (room conditions)
rec	Receiver
sat	Saturation temperature
sf	Surface
sys	System
v	Vapor
V	Volume
w	Wall

Greek symbols

Δ	Change
ε	Emissivity
η	Efficiency
λ	Wavelength, nm
ρ	Density, kg/m^3
σ	Extinction coefficient, 1/cm

[1] M. Thirugnanasambandam, S. Iniyan, and G. Ranko, Renew. Sustain. Energy Rev. **14** (2010).
[2] A. J. Hunt, Lawrence Berkeley Laboratory Report No. LBL-7841, 1978.
[3] M. Abdelrahman, P. Fumeaux, and P. Suter, Sol. Energy **22** (1979).
[4] F. J. Miller and R. W. Koenigsdorff, J. Sol. Energy Eng. **122** (2000).
[5] R. Bertocchi, J. Karni, and A. Kribus, Energy **126**, 29 (2004).
[6] S. Haussener, D. Hirsch, C. Perkins, A. Weimer, A. Lewandowski, and A. Steinfeld, J. Sol. Energy Eng. **131** (2009).
[7] L. O. Schunk, P. Haeberling, S. Wepf, D. Wuillemin, A. Meier, and A. Steinfeld, J. Sol. Energy Eng. **130** (2008).
[8] N. Arai, Y. Itaya, and M. Hasatani, Sol. Energy **32** (1984).
[9] A. Z'Graggen and A. Steinfeld, Int. J. Heat Mass Transfer **52** (2009).
[10] X.-Q. Wang and A. S. Mujumdar, Int. J. Therm. Sci. **46** (2007).
[11] S. Choi, D. A. Siginer, and H. P. Wang, *Developments and Applications of Non-Newtonian Flows* (ASME, New York, 1995), FED-Vol. 231; MD-Vol. 66.
[12] H. Kim, J. Kim, and M. Kim, Int. J. Multiphase Flow **33**, 7 (2007).
[13] I. C. Bang and S. H. Chang, Int. J. Heat Mass Transfer **48**, 12 (2005).
[14] W. J. Minkowycz, E. M. Sparrow, R. J. Goldstein, W. E. Ibele, E. Pfender, and P. L. Blackshear, Jr., Int. Commun. Heat Mass Transfer **33**, 4 (2006).
[15] J. B. Gadhe and R. B. Gupta, Int. J. Hydrogen Energy **32** (2007).
[16] D. W. Zhou, Int. J. Heat Mass Transfer **47**, 3109 (2004).
[17] D. Wen and Y. Ding, Int. J. Heat Mass Transfer **47**, 5181 (2004).
[18] T. Otanicar, R. A. Taylor, P. E. Phelan, and R. Prasher, Proceedings of the Third International Conference on Energy Sustainability, 2009.
[19] H. Tyagi, P. E. Phelan, and R. Prasher, J. Sol. Energy Eng. **131**, 4 (2009).
[20] P. E. Phelan, P. Bhattacharya, and R. Prasher, Annu. Rev. Heat Transfer **14** (2005).
[21] MTI, Nanopowders: A-Z, http://www.mtixtl.com/nanopowdersa-z.aspx (accessed January 2011).
[22] S. A. Kumar, K. S. Meenakshi, B. R. V. Narashimhan, S. Srikanth, and G. Arthanareeswaran, Mater. Chem. Phys. **113** (2009).
[23] H. Chang and Y. Chang, J. Mater. Process. Technol. **207** (2008).
[24] Edmund Optics, http://www.edmundoptics.com/ (accessed January 2011).
[25] Solutia, Therminol VP-1, http://www.therminol.com/pages/products/vp-1.asp (accessed July 10, 2010).
[26] M. F. Modest, *Radiative Heat Transfer*, 2nd ed. (Academic, Reading, MA, 2003).
[27] R. B. Pettit and R. R. Sowell, J. Vac. Sci. Technol. **13** (1976).
[28] W. B. Stine and R. B. Driver, Sandia National Laboratories—available online at http://handle.dtic.mil.ezproxy1.lib.asu.edu/100.2/ADA353041 (1994).
[29] S. Kumar and C. L. Tien, National Heat Transfer Conference, 1989.
[30] Abengoa Solar, http://www.abengoasolar.com/corp/export/sites/solar/resources/pdf/en/PS10.pdf (accessed January 2011).
[31] T. Otanicar, P. E. Phelan, R. S. Prasher, G. Rosengarten, and R. A. Taylor, J. Renewable Sustainable Energy **2** (2010).
[32] NREL, 30-Year Average Monthly Solar Radiation, http://rredc.nrel.gov/solar/old_data/nsrdb/1961-1990/redbook/sum2/state.html (accessed January 2011).
[33] S. Kaplan, CRS Report for Congress, http://www.fas.org/sgp/crs/misc/RL34746.pdf (accessed January 2011).